NeuroImage 83 (2013) 458–471

Contents lists available at ScienceDirect

NeuroImage

journal homepage: www.elsevier.com/locate/ynimg

Stimulus detection rate and latency, firing rates and 1–40 Hz oscillatory power are modulated by infra-slow fluctuations in a bistable attractor network model

Mikael Lundqvist [a,b,*,1], Pawel Herman [a,b,1], Matias Palva [c], Satu Palva [c], David Silverstein [a,b], Anders Lansner [a,b]

[a] Department of Computational Biology, Royal Institute of Technology (KTH), Sweden
[b] Stockholm University, Sweden
[c] Neuroscience Center, University of Helsinki, Finland

ARTICLE INFO

Article history:
Accepted 30 June 2013
Available online 10 July 2013

Keywords:
Slow fluctuation
Oscillation
Attractor network
Threshold-stimulus detection task
Computational model
Detection rate

ABSTRACT

Recordings of membrane and field potentials, firing rates, and oscillation amplitude dynamics show that neuronal activity levels in cortical and subcortical structures exhibit infra-slow fluctuations (ISFs) on time scales from seconds to hundreds of seconds. Similar ISFs are salient also in blood-oxygenation-level dependent (BOLD) signals as well as in psychophysical time series. Functional consequences of ISFs are not fully understood. Here, they were investigated along with dynamical implications of ISFs in large-scale simulations of cortical network activity. For this purpose, a biophysically detailed hierarchical attractor network model displaying bistability and operating in an oscillatory regime was used. ISFs were imposed as slow fluctuations in either the amplitude or frequency of fast synaptic noise. We found that both mechanisms produced an ISF component in the synthetic local field potentials (LFPs) and modulated the power of 1–40 Hz oscillations. Crucially, in a simulated threshold-stimulus detection task (TSDT), these ISFs were strongly correlated with stimulus detection probabilities and latencies. The results thus show that several phenomena observed in many empirical studies emerge concurrently in the model dynamics, which yields mechanistic insight into how infra-slow excitability fluctuations in large-scale neuronal networks may modulate fast oscillations and perceptual processing. The model also makes several novel predictions that can be experimentally tested in future studies.

Introduction

Infra-slow (~0.01−0.1 Hz) fluctuations (ISFs) are a pervasive feature of spontaneous mammalian brain activity (Palva and Palva, 2012). At the single-neuron level, ISFs characterize the firing rates of neurons in, for instance, thalamus (Albrecht and Gabriel, 1994; Werner and Mountcastle, 1963) and basal ganglia (Allers et al., 2002). These firing rate fluctuations are correlated with infra-slow amplitude modulations of fast theta- (4–8 Hz) (Allers et al., 2002) and alpha-band (8–14 Hz) (Hughes et al., 2011) oscillations in field potential recordings. Generally, ISFs are prominent in direct recordings of spontaneous cortical activity (Leopold et al., 2003; Nir et al., 2008) and in non-invasive magnetoencephalography (MEG) recordings of ongoing human brain activity (Linkenkaer-Hansen et al., 2001). ISFs are salient also in the blood-oxygenation-level dependent (BOLD) signals (Biswal et al., 1995) and are correlated between anatomically distributed brain regions that form functionally distinct brain systems (Fransson, 2005; Greicius et al., 2003; Power et al., 2011). The BOLD ISFs are directly correlated with ISFs in 1–100 Hz EEG and oscillatory power of local field potentials (LFPs) (Goldman et al., 2002; Leopold et al., 2003; Mantini et al., 2007) and, in addition, MEG-recorded amplitude dynamics and BOLD-ISFs have similar anatomical patterns of temporal correlations (Brookes et al., 2011). Furthermore, ISFs are observable directly in neuronal membrane potentials (Lörincz et al., 2009), cortical potentials (Aladjalova, 1957; Norton and Jewett, 1965) and in human EEG (Monto et al., 2008; Vanhatalo et al., 2004). Importantly, they are correlated both with >1-Hz oscillation amplitudes and psychophysical performance fluctuations (Monto et al., 2008). Also, bistable switching between low and high amplitude modes of EEG alpha oscillations on a comparably slow time scale has recently been reported (Freyer et al., 2009).

* Corresponding author at: Department of Computational Biology, Royal Institute of Technology and Stockholm University, Roslagstullsbacken 35, 11421 Stockholm, Sweden.
E-mail address: lundqvis@csc.kth.se (M. Lundqvist).
[1] Contributed equally to this work and should be both considered as first authors.

1053-8119 © 2013 The Authors. Published by Elsevier Inc. Open access under CC BY-NC-SA license.
http://dx.doi.org/10.1016/j.neuroimage.2013.06.080

ISFs are thus a widespread phenomenon but surprisingly little is known about the mechanisms underlying their generation and, in particular, mediating their functional consequences. Modeling studies have typically been focused on their genesis (Deco and Jirsa, 2012; Deco et al., 2009; Ghosh et al., 2008; Honey et al., 2007). Common for these models is that they operate close to a critical point at the edge of stability, a regime that has been linked to cortical dynamics in earlier models (Robinson et al., 1997, 2001). Self-organized criticality has accordingly been proposed to underlie experimentally observed long-range temporal correlations of fast oscillations and to be crucial for the generation of ISFs (Linkenkaer-Hansen et al., 2001). In vitro recordings, on the other hand, have demonstrated that astrocytic Ca^{2+} oscillations are associated with periodic ATP release and hyperpolarizing potentials in neurons, and thereby directly underlie the generation of ISFs both in the neuronal firing rates and oscillation amplitudes (Lörincz et al., 2009).

Here, we rather address the functional implications of imposed ISFs in synaptic background noise that could conceivably arise through any of the aforementioned mechanisms. We employ a hierarchical modular cortical attractor network structure (Djurfeldt et al., 2008; Lundqvist et al., 2006, 2010) comprising more than 30,000 Hodgkin–Huxley type cells distributed in two patches. The attractor dynamics of this network with a stable ground state and stimulus-triggered retrieval of memory patterns stored in the recurrent connections is used as a model for stimulus detection. This approach allows us to explicitly address the effects of ISFs both on the amplitude dynamics of 1–40 Hz oscillations and also on stimulus detection probabilities and latencies. Consistently with experimental data (Albrecht and Gabriel, 1994; Allers et al., 2002; Lörincz et al., 2009; Monto et al., 2008; Nir et al., 2008; Ruskin et al., 2003; Vanhatalo et al., 2004; Werner and Mountcastle, 1963), the simulated ISFs modulate the firing rates, amplitudes of fast neuronal oscillations and the probability of detecting sensory stimuli. In addition, the model predicts that detection latency as well as the peak frequency of alpha oscillations should be modulated by ISFs, and that simultaneous bursts in delta/theta and upper beta/gamma bands should accompany detected stimuli.

Methods

Network model

We used a biophysically detailed network model of cortical layer 2/3 developed earlier (Djurfeldt et al., 2008; Lundqvist et al., 2006, 2010) and now translated (Silverstein and Lansner, 2011) to the parallel NEURON simulator (Carnevale and Hines, 2006). Simulations were performed on a supercomputer with a 128-node partition in virtual node mode, providing 256 processors, each of which ran one message passing interface (MPI) process simulating a single minicolumn. Each cortical simulation was typically run for 100 s of cortical activity with a fixed simulation time step of 50 μs.

The model had both hypercolumnar and minicolumnar organizations (Fig. 1A). Each layer 2/3 portion of a minicolumn contained 30 pyramidal cells (Peters and Yilmaz, 1993) and one basket cell. Each minicolumn also included a rudimentary layer 4, with 5 pyramidal cells transmitting simulated sensory input in a feedforward fashion to layer 2/3. The connectivity was defined as the probability, P, that a cell in the pre-synaptic population was connected to a cell in the post-synaptic population. In consequence, it served as the estimate of the percentage of cells in the pre-synaptic population that are connected to the post-synaptic population. Each layer 4 cell randomly connected to the layer 2/3 pyramidal cells with $P = 0.5$ in the same minicolumn, while the layer 2/3 cells formed recurrent connections ($P = 0.25$) within each minicolumn.

Every hypercolumn contained 49 such minicolumns and a pool of 49 basket cells. These basket cells provided feedback inhibition to all the minicolumns within each hypercolumn, consistent with the finding that parvalbumin-positive interneurons in layer 2/3 provide non-specific inhibition within a few hundred microns while pyramidal cells form smaller, interconnected clusters in this volume (Kampa et al., 2006; Yoshimura et al., 2005). The hypercolumns were assumed to have strict borders in the sense that all basket cells were connected to minicolumns within their hypercolumn and to none outside (Fig. 1A). We did however perform simulations removing this constraint using a setup where the extent of feedback inhibition was determined by the geometrical position rather than predefined hypercolumn identity (see section Continuous hypercolumns).

A cortical patch was represented by 9 hypercolumns. In total, 49 non-overlapping attractor memory patterns were stored by means of selective sparse long-range connectivity between minicolumns from separate hypercolumns (c.f. Figs. 1A and B). This connectivity was set manually prior to a simulation by selecting a single unique minicolumn in each hypercolumn to constitute a specific distributed pattern and by adding reciprocal connections between the selected minicolumns. Each pattern was thus composed of 9 unique minicolumns. On a single cell level these long-range pyramidal–pyramidal connections had a fixed probability ($P = 0.3$) for cells sharing a pattern and zero probability otherwise. Further, the synaptic strengths were identical for all long-range connections (Fig. 1A).

The minicolumns had a diameter of 30 μm and were closely packed on a two-dimensional square grid with 1.5 mm side. All pyramidal cells in a minicolumn shared the same x and y coordinates but were uniquely spread out on the z-axis along 500 μm. Interneurons were placed near the center of each minicolumn with respect to the z-axis. Synaptic conductances and connectivity were compatible with biological data (Thomson et al., 2002; c.f. Lundqvist et al., 2006). In simulations of the two-patch model, there was a hierarchical organization of two identical, connected networks where the first patch (receiving external input, see below) acted as a "lower-order" network and the other acted as an "associative" network later in the input stream (Fig. 1B), receiving sensory input indirectly via feedforward connections from the first network. These feedforward projections were local in the sense that a specific minicolumn in the associative network only received input from its twin minicolumn in the lower-order network. Each pyramidal cell in the sending minicolumn connected with $P = 0.1$ to the cells selected randomly in the receiving minicolumn, and the conductance for each connection was half of the conductance used in the local connections within the minicolumn (except when otherwise stated). Each cell in the associative network therefore received on average only 3 connections from the lower-order network compared to ~90 recurrent connections from other cells in the associative network. Taking connection strengths and their number into account the ratio between inter- and intra-patch excitation was roughly 0.1. Single minicolumns in the lower-order network could be selectively stimulated by pyramidal cells mimicking layer 4 input cells. These were activated by spike trains generated by Poisson processes such that they produced 2–3 spikes during 30 ms of stimulation. Typically, 4 out of 9 minicolumns in a distributed attractor pattern were stimulated in such a manner.

All conduction delays within a patch were calculated assuming a conduction speed of 0.5 m/s, while projections between patches had velocities of 2.5 m/s (Girard et al., 2001).

Continuous hypercolumns

In the version of the model referred to as a continuous hypercolumn model, we laid out all 441 minicolumns of each cortical patch on a row with one basket cell close to each minicolumn (Fig. 1C). Pyramidal cells in a given minicolumn were connected ($P = 0.7$) to the 25 closest basket cells (12 in each direction plus the basket cell directly adjacent to the minicolumn). Basket cells

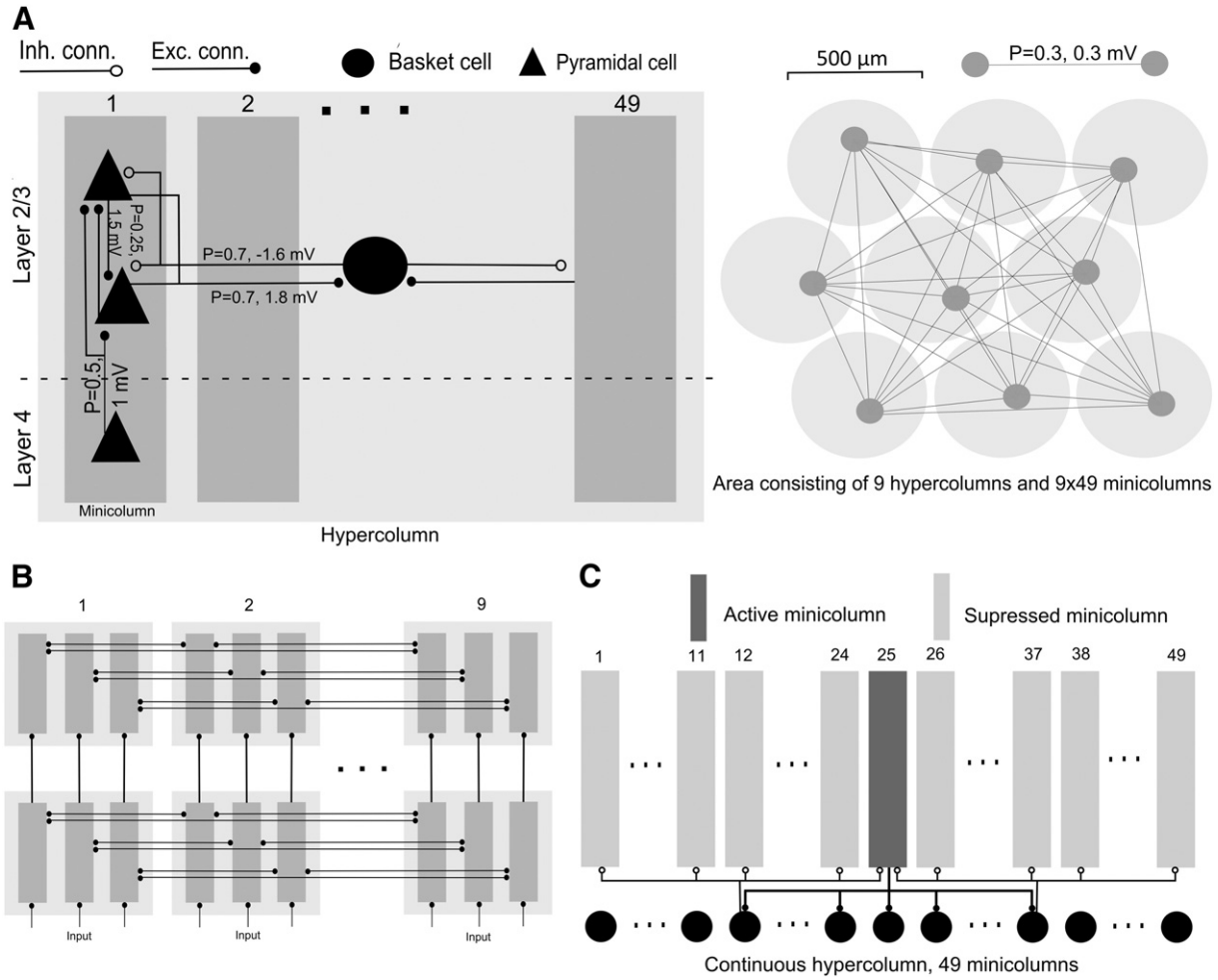

Fig. 1. Network setup and connectivity. A: A detailed connectivity of a single hypercolumn, containing 49 minicolumns, seen from the side (left) and a sketch of the long-range connectivity within a cortical area (right), consisting of 9 such hypercolumns, seen from above. The numbers on the arrows describe the connectivity and the size of postsynaptic potential (PSP) at resting potential of the postsynaptic cell. Connectivity is given as the probability that a given cell in the pre-population connects to a specific cell in the post-population. B: Global connections between and within the two areas. Area 1 (sensory area) receives external input which is then transmitted to area 2 (associative area). Each minicolumn in area 1 has feed-forward connections only to the closest minicolumn in the above area (10% connectivity and an EPSP of 0.8 mV) and also share attractor activity pattern with it. C: Model with continuous hypercolumns that emerge dynamically around active minicolumns. Here one such hypercolumn is depicted. It is comprised of one active minicolumn (dark gray rectangle) and 48 adjacent minicolumns (light gray rectangles) that are disynaptically suppressed via basket cells (black circles). The connections marked with filled circles represent excitatory connections, while inhibitory connections are marked with open circles.

were also connected to pyramidal cells (P = 0.7) in the 25 closest minicolumns in the same fashion. This meant that a minicolumn could provide di-synaptic inhibition onto the 49 closest minicolumns, including itself (Fig. 1C). In Fig. 1C, minicolumn 25 is active and suppresses minicolumns 1–49, hence defining a hypercolumn. If minicolumn 26 became active instead, the hypercolumn would be comprised of minicolumns 2–50. In this setup we could use the same parameters and also local as well as global connection matrices between pyramidal cells. The only difference was a 30% reduction in the conductance of pyramidal-basket cell connections to retain similar excitation levels.

Cell model

Relative to previous studies (Lundqvist et al., 2006, 2010), the second type of interneurons, regular spiking non-pyramidal (RSNP) cells, were removed since they did not produce any qualitative difference for the results presented here. The cells included were layer 2/3 pyramidal cells and soma targeting basket cells assumed to correspond to fast spiking cells. As in earlier studies (Fransén and Lansner, 1995), the model neurons were multi-compartmental and conductance-based, following the Hodgkin–Huxley and Rall formalisms. In short, pyramidal cells had 6 compartments (soma, basal dendritic, initial segment, and three apical dendritic) and interneurons had 3 (soma, dendritic, and initial segment). The potential E in a compartment was calculated by integrating the currents

$$\frac{dE}{dt} = \frac{(E_{leak} - E)g_m + \sum\left(E_{comp} - E\right)g_{core} + (E_{ex} - E)g_{ext} + I_{channels} + I_{syn} + I_{inj}}{c_m} \tag{1}$$

where c_m is the capacitance of the membrane, g_m is the membrane leak conductance, E_{leak} is the equilibrium potential of the leak current, and g_{core} is the core conductance between connected compartments, which is dependent on compartmental cross section (equal for basal and apical dendrites, smaller for initial segment). g_{ext} is a non-specific excitatory conductance with reversal potential E_{ex}, $I_{channels}$ is the active currents from the different ionic channels in the membrane of the compartment, including voltage-dependent Na^+, K^+, and Ca^{2+} channels as well as Ca^{2+}-dependent K^+ channels. I_{syn} is the current through glutamatergic and GABA-ergic synapses on the compartment and I_{inj} is the injected current. For individual cells of a certain type all parameters were fixed except size, which varied ±10% according to a uniform

distribution. Pyramidal cells were strongly adapting due to the Ca^{2+}-dependent K^+ channels which caused attractors to have finite life-time (Fig. 2). The decay time constant for the Ca^{2+} was 1 s. For complete synapse and model equations, see Silverstein and Lansner (2011).

Synapse model

Pyramidal-to-pyramidal connections had both AMPA and voltage-dependent NMDA components. Synapses formed by pyramidal cells onto basket cells were purely AMPA-mediated while the inhibitory cells formed $GABA_A$-type synapses. Global connections and excitatory noise synapses were placed on the second apical dendritic compartment and local connections from cells in the same minicolumn were placed on the basal dendritic compartment. The inhibitory basket cells connected to the soma. Time constants for the different synapses were $\tau_{AMPA} = 6$ ms, $\tau_{GABA} = 6$ ms and $\tau_{NMDA} = 150$ ms. All pyramidal-to-pyramidal connections were depressing. Depression was multiplicative (Tsodyks et al., 1998), decreasing the synaptic conductance of the synapse 25% with each incoming spike and decaying back to the initial conductance with a time constant of 700 ms.

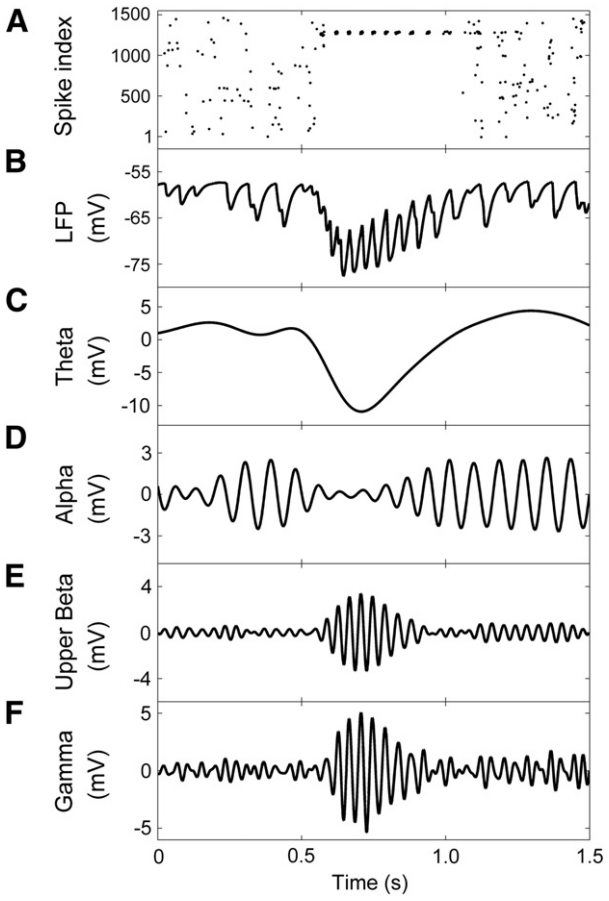

Fig. 2. Spiking and oscillatory behavior in the two network states, non-coding ground state and coding attractor state. The spiking activity (A) of pyramidal cells within a single hypercolumn is shown. At the start of the simulation the network is in its non-coding ground state. A stimulus triggered activation of one of the network's attractors causes increased firing rates in the cells belonging to the minicolumn which constitutes a part of the activated attractor pattern in each hypercolumn whereas cells in the remaining minicolumns fire at reduced rates (here, hardly any firing in those background minicolumns is seen). This activation of the attractor pattern is accompanied by a switch in the oscillatory dynamics of the synthesized LFP (B), from the ground state alpha (D) to gamma oscillations (F). The gamma rhythm (F) is nested on the delta/theta wave (C) associated with the activation–deactivation cycle of the attractor pattern with finite lifetime (here ~500 ms).

Noise fluctuations as a model for ISF generation

The pyramidal cells in layer 2/3 received noisy background excitation through low-conductance AMPA synapses (0.1 mV EPSP, ~15 times smaller than local pyr–pyr conduction) activated by simulated Poisson spike trains with an average firing rate of 300 s^{-1} (called noisy excitation for the reminder of the paper). This background noise represented activity of connected neurons outside the simulated cortical patch. Each pyramidal cell received an individual Poisson spike train. This source alone made the pyramidal cells spike at ~0.8 s^{-1} (c.f. top panel in Fig. 5A). ISFs were imposed on the network by modulating the conductance of noisy excitation with a sinusoidal wave that decreased and increased the noise conductance by a maximum of 10% and with a period of 10 s. Alternatively, the frequency of the spike trains generated by the background noise was modulated with a smooth step function (exponential rise and fall with short time constants) resulting in alternating switches between the baseline and elevated (110%) rate, both lasting ~10 s. The imposed ISFs thus reflected slow fluctuations in the activity of the global network in which the simulated patches were assumed to be submerged.

In some simulations we removed the fluctuating component of the noisy excitation and instead examined the performance of the network under different stationary conditions (i.e. constant within each trial). This allowed for emulating conditions analogous to a specific ISF phase in previous experiments but lasting throughout an entire simulation trial.

Attractors, bistability and oscillations

The network operated in a bistable regime (Amit and Brunel, 1997; Lundqvist et al., 2010) with two distinct dynamical states having attractor characteristics — a so-called non-coding ground state and active coding state. This regime was present for a specific balance between excitation and inhibition (Amit and Brunel, 1997), but it did not require parameter fine-tuning of the network due to the modular structure (Lundqvist et al., 2010). The non-coding ground state was the default state of the network with all pyramidal cells active at a very low rate. Following specific, external stimulation the network could end up in the coding attractor state, where a cell assembly constituting the attractor associated with the stimulus was activated. Considering there are several such stable coding attractors in the network, similar networks are sometimes described as multistable. Here, however, we consistently use the term bistable to emphasize the distinct dynamical and functional nature of the two aforementioned network states.

Each coding attractor was manifested as a sparse and distributed pattern with a single active minicolumn (elevated firing rates) in every hypercolumn and the remaining 48 minicolumns being almost silent. In each hypercolumn basket cell feedback inhibition (Fig. 1A) provided competition between the minicolumns. In the non-coding ground state this negative feedback reduced the firing rates of all pyramidal cells and introduced oscillations in population activity and membrane potentials at ~8–12 Hz (Fig. 2). Following stimulation, the feedback inhibition acted as a winner-take-all mechanism within each hypercolumn, where one minicolumn (the active one, i.e. belonging to the activated pattern) was spiking at an elevated rate and the rest at reduced rates. Due to cellular adaptation and synaptic depression the coding attractor states had limited life-time (Lundqvist et al., 2006); without these mechanisms the coding attractors would have been persistent (Lundqvist et al., 2010). As a result, the activation of an attractor produced a delta/theta wave carrying nested faster gamma-like oscillations (Fig. 2). Dendritic targeting interneurons (Klausberger and Somogyi, 2008; Rotstein et al., 2005; White et al., 2000) could also contribute to the theta rhythm emerging in the network with the activation of short-lived attractors, as recently demonstrated by Krishnamurthy et al. (2012).

Detection rate and latency

In order to categorize a stimulus as detected (hit) or not (miss) we examined the distribution of spikes generated in layer 2/3 cells in the associative-patch network. The necessary condition for a hit was the activation of all the minicolumns in the partially stimulated attractor pattern. The activation criterion for a minicolumn was the generation of at least 40% of all spikes from pyramidal cells in the respective hypercolumn within any sliding window of 150–200 ms in the period up to 500 ms after stimulation (100 ms delay was added for the analysis in the higher area). The detection rate (hit rate) was defined as the percentage of successfully detected stimulations averaged over 10 trials. In each trial, 100 stimulations were applied at a rate of 1 s^{-1}.

The detection latency in the network was determined based on the analysis of the spike time distributions for detected patterns. In particular, it was defined as the estimate of the latency of a prominent early peak in the distribution.

Synthetic local field potentials

LFPs were estimated by calculating the average soma potential for all cells in a local population (minicolumn) at every time step, similarly to the approach adopted by Ursino and La Cara (2006). Although LFP is more directly linked to the synaptic activity, the averaged membrane potentials have been reported to be highly correlated with LFPs and to have similar information content (Okun et al., 2010). Here we used the global LFP averaged over the 9 hypercolumns within each cortical patch.

Spectral and phase analysis

All analyses of area-averaged LFPs were performed using MATLAB (with the support of FieldTrip toolbox for multitaper spectral estimation Oostenveld et al., 2011). LFPs were produced at the sampling frequency of 1 kHz. We designed band-pass filters to extract specific frequency components. Since the causal filters introduce a delay, we applied them both in the forward and reverse directions by switching the sequential order of signal samples to counteract the resultant phase shift and obtain the effect of zero-phase filtering.

The power spectra of LFP trials were obtained using the multitaper method (Thomson, 1982), with a family of orthogonal tapers produced by Slepian functions (Slepian and Pollak, 1961). This approach reduces spectral estimation bias and variance by averaging statistically independent estimates obtained from tapered (windowed) data, hence allowing for robust control of the frequency smoothing. The number of tapers, determined by the amount of time and frequency smoothing, depended on the frequency range being examined. On average, for low frequencies up to 5 Hz the time window was set to fit at least 5 cycles. For the mid-range, roughly from 5 to 20 Hz, at least 8 cycles were fit within the window span. Finally, for higher frequencies the time windows were adjusted to account for 12 or more full cycles. Overall, the time-bandwidth product was kept around 2. The power spectra for the entire LFP trial were extracted through averaging the time–frequency representations over quasi-stationary time intervals.

Additionally, a nesting relationship between ISF and 1–40 Hz oscillations was examined by analyzing phase–amplitude coupling effects (Monto et al., 2008; Vanhatalo et al., 2004). At first, LFPs were band-pass filtered to extract ISF (below 0.1 Hz), theta (1–5 Hz, θ), alpha (8–15 Hz, α), upper beta (22–28 Hz, β) and gamma rhythms (30–40 Hz, γ). Then, their analytic representations (without negative frequency components usually seen in Fourier spectra of real-valued signals) were extracted by applying a Hilbert transform. The amplitude envelopes of 1–40 Hz components (magnitudes of the corresponding complex analytic signals), $env_{\theta/\alpha/\beta/\gamma}$, were next filtered using the same filter that was applied to separate the ISF (filter with the cut-off frequency below 0.1 Hz). Finally, 1:1 phase synchrony between the instantaneous phase of the resultant ISF-filtered envelopes, $\Phi_{env}(t)$, and that of the ISF signal, $\Phi_{ISF}(t)$, was estimated to quantify the strength of ISF-phase modulation of theta, alpha, beta and gamma amplitudes (phase–amplitude coupling). The phase synchrony was evaluated in this case using the following phase-locking value (PLV_{PAC}) (Lachaux et al., 1999; Vanhatalo et al., 2004):

$$PLV_{PAC} = \frac{1}{N}\left|\sum_{k=1}^{N} \exp(j(\Phi_{ISF}(t_k) - \Phi_{env}(t_k)))\right|,$$

where N is the number of samples. Due to the length of the ISF cycle we used the entire 100-s-long trials for estimation, i.e. 100,000 samples. The quantities reported in this study are values averaged over 10 trials. To complement the analysis of nesting phenomena, we also applied the envelope-to-signal correlation (ESC) method of Bruns and Eckhorn (2004). In short, the ESC measure is defined as the correlation between a narrow-band low-frequency signal (here: ISF component), x_{ISF}, and the amplitude envelope of a faster rhythm (here: θ, α, β and γ oscillatory components), $env_{\theta/\alpha/\beta/\gamma}$:

$$ESC = \mathrm{Corr}\left(x_{ISF}(t), env_{\theta/\alpha/\beta/\gamma}(t)\right).$$

When compared to PLV_{PAC}, ESC provides information about the positive or negative nature of amplitude correlations and is more sensitive to specific configurations of the alignment between the phase of a slow modulating rhythm and the amplitude of faster oscillations.

Spike-field coupling in the analysis of the distribution of spikes produced by pyramidal and basket cells during ongoing alpha oscillations in the network's non-coding ground state was quantified by applying a point-field phase synchronization measure that captures the consistency of spike-LFP phases in the alpha band within a trial (Vinck et al., 2011). In particular, we employed the mean PLV, where instead of the phase difference argument in the original formulation (c.f. PLV formula above for a pair of phase series) we used the series of alpha phases, Φ_{α}, corresponding to spike events. In addition, a two-sample Watson–Williams test (cf. Fisher, 1995) was performed to assess if the means of the two phase distributions, corresponding to spikes produced by pyramidal and basket cells, were identical. This statistical evaluation was preceded by a Rayleigh test to verify unimodal deviation from uniformity in the phase distribution (cf. Fisher, 1995).

Results

We addressed here the effects of ISFs on stimulus detection rate (hit rate) and latency (detection time) as well as fast oscillations in a large-scale cortical network simulation of neuronal activity during a threshold-stimulus detection task (TSDT) (Linkenkaer-Hansen et al., 2004; Monto et al., 2008; S. Palva et al., 2005; Sadaghiani et al., 2010). Two alternative models of imposed infra-slow modulation of background noise giving rise to ISFs were examined: (*i*) a slow sinusoidal fluctuation in excitatory noise conductance or (*ii*) fast switching between two long-lasting levels of spike rate of excitatory background noise (Methods section). Cortical activity was simulated in a layer 2/3 network model (Fig. 1) with a number of stored attractor patterns (Methods section), which allowed for emulating a TSDT. These attractors could be fully activated by partial stimulation, which was then interpreted as a successful detection. Once activated they persisted longer than stimulus duration (c.f. Fig. 2 where stimulation is 30 ms and the corresponding pattern is active for ~400 ms, please see also Lundqvist et al., 2006). Brief and weak stimulations were provided and the response of the network was quantified in terms of spiking activity, oscillatory dynamics of synthesized LFPs, hit rate and detection time. The stimulus strength was set so that the network

detected roughly 50% of all the stimuli. The default model had a hierarchical structure representing two connected cortical patches: a lower-order network and an associative network corresponding to a higher-level cortical region that received its only inputs from the lower-order patch (Fig. 1B). This organization was motivated by the fact that the unperceived stimuli in TSDTs evoke only local activity in early sensory regions whereas consciously perceived stimuli are associated with global-scale network engagement (S. Palva et al., 2005). Additionally, activation or entrainment of brain areas higher up in the processing hierarchy has been suggested to be essential for conscious perception (Dehaene and Changeux, 2011; Dehaene et al., 2006). We therefore presented the stimuli to the lower-level network and used full activation (Methods section) of the corresponding pattern in the higher-level network as a criterion for stimulus detection. Before reporting the results of our TSDT simulations under the ISF condition we first describe some fundamental characteristics of the single-patch network as well as the full network in the absence of ISFs.

Basic behavior of the network in the absence of ISFs

Each cortical patch was a copy of a previously developed layer 2/3 attractor network (Djurfeldt et al., 2008; Lundqvist et al., 2006, 2010) with 15,876 pyramidal neurons arranged into a hypercolumnar and minicolumnar structure (Figs. 1A,B), with a total of 441 minicolumns divided into 9 hypercolumns. The network had two simultaneously stable states (Amit and Brunel, 1997) and by default it was in the non-coding ground state. Upon successful stimulus detection associated with the retrieval of the corresponding attractor memory, the network switched to a coding attractor state where the subset of cells belonging to the stimulated pattern became active with firing at an elevated rate (Fig. 2 top panel and Methods section). Neural adaptation and synaptic depression caused the activated attractors to have a finite life-time, which gave rise to a transient delta/theta wave (Fig. 2C) in the synthetic LFP (Fig. 2B) (Lundqvist et al., 2011). In addition, the pyramidal-basket-cell loop resulted in pulsed inhibition (Brunel and Hakim, 1999; Whittington et al., 2000) released periodically on the pyramidal cells within each hypercolumn. This was crucial for generating the gamma- (Fig. 2F) and upper-beta-band (Fig. 2E) oscillations, which shared dynamical properties and were nested in the theta cycle. Overall, during the simulated TSDT, the power spectra of the synthesized and spatially averaged LFP in each patch (Fig. 3A) were qualitatively similar to those reported for human MEG and EEG (Linkenkaer-Hansen et al., 2004; Monto et al., 2008) with the dominant alpha component, which suggested prima facie validity of the model.

The network also displayed oscillations in alpha band. This rhythm emerged in the cortical patch (Fig. 2D) as a result of the network dynamics in the non-coding ground state (Djurfeldt et al., 2008; Lundqvist et al., 2010, 2011). It was dependent on the same excitatory–inhibitory loop that generated gamma/upper beta oscillations during attractor retrieval, i.e. reciprocal interaction between pyramidal and basket cell populations firing at distinct phases (Watson–Williams test, $P < 0.01$) of the alpha cycle (compare upper and lower panels in Fig. 3B). The difference in the frequency between the characteristic oscillations in two states was due to inherently lower overall level of excitation in the non-coding state accompanied by low firing rates (Lundqvist et al., 2010). The characteristic dominance of the alpha component in the power spectrum was observed mainly due to the fact that the network spent a majority of the simulation time in the alpha-generating ground state.

The ground state alpha-like oscillations emerged in the synthetic LFP when the noisy excitation was set above a threshold level separating the oscillatory from the non-oscillatory regime (cyan curve in Fig. 3C corresponding to 90% noisy excitation level). Just above this threshold the oscillations had a peak frequency of ~8–9 Hz. Increasing the noisy excitation further enhanced the amplitude and peak frequency (Fig. 3C). The general band power increase with noisy excitation was explained by changes in the firing patterns. Spiking was extremely sparse in the ground state and only a small fraction of pyramidal and basket cells fired in each alpha cycle. When the noisy excitation was strengthened the average number of cells firing per cycle increased. This led to deepening of the trough of the cycle, reflecting the contribution of enhanced basket cell firing (Fig. 3D, red dots), which resulted in a locally-linear increase of the alpha-band power with noisy excitation (Fig. 3D, blue circles). A strong correlation between the number of pyramidal and basket cell spikes ($r^2 = 0.98$, $P < 0.01$) ensured dynamical regulation of the excitation–inhibition balance in the ground state. The proportion of pyramidal cells locked to the alpha rhythm rose with increased background excitation, as demonstrated by the distribution of the number of spikes corresponding to different alpha phases for two excitation levels (Fig. 3E). In consequence, enhanced spike-field coupling could be observed (two-fold increase in phase consistency evaluated using PLV, Methods section).

In addition, we studied how the range of recurrent excitation allowing for simultaneous stable ground state dynamics and retrievable attractor patterns, was affected by changes in noisy excitation. This so-called bistable range (Methods section), and particularly its upper boundary (Fig. 3F, blue curve), decreased as the noisy excitation increased. Above this boundary the coding attractors activated spontaneously at the cost of the ground state. As can be seen from the blue curve in Fig. 3F, this occurred for progressively lower values of recurrent excitation as the noisy excitation was increased.

Finally, we investigated the interaction of the two networks in a hierarchical model and found that even with feedforward inter-patch connections, which were much weaker than the recurrent intra-areal connections (Fig. 1B; Methods section), the associative network was still more responsive to stimulations than the lower-order network. When a weak stimulus was applied, even partial activation of the memory pattern in the lower-order network was sufficient for a successful detection (retrieval of the entire memory pattern) in the associative network. In consequence, the hit rate obtained in the associative network was higher than in the lower-order network and strongly modulated by the projection strength between the patches (Fig. 4, compare blue and red bars).

ISFs are correlated with stimulus detection rate and latency

We imposed slow fluctuations in the synaptic conductance of noisy excitation, reflecting background activity of the global network in which the simulated patches were assumed to be submerged. We then examined whether this produced an ISF (Biswal et al., 1995; Monto et al., 2008; Nir et al., 2008; Penttonen et al., 1999) in the synthetic LFP measured in the two patches. In particular, we added a sine wave component to the stationary pyramidal cell noise conductance with a period of 10 s and peak amplitude corresponding to 10% of its baseline level, which limited the alpha peak frequency to vary between 8 and 12 Hz (as can be deduced from 90 and 110% noise levels in Fig. 3C). As expected, this fluctuation in conductance indeed led to the generation of a pronounced 0.1-Hz component in the patch-averaged LFP (black line in the bottom panel of Fig. 5A). On the other hand, when all recurrent connectivity in the network was removed, the ISF seen in LFP was strongly dampened, its phase was reversed (red line in the bottom panel of Fig. 5A) and firing rate fluctuations significantly increased (red line in the top panel of Fig. 5A). This implies that the net effect of increased noisy excitation was in fact inhibitory in the intact network and therefore the ISF trough occurred when the noisy excitation was at its peak. This inhibitory effect can also be seen in the modulation of basket cell firing rates. During periods of high excitatory drive the average membrane potential of pyramidal cells in the network was reduced due to the recruitment of basket cells (blue line in the top panel of Fig. 5A), which effectively

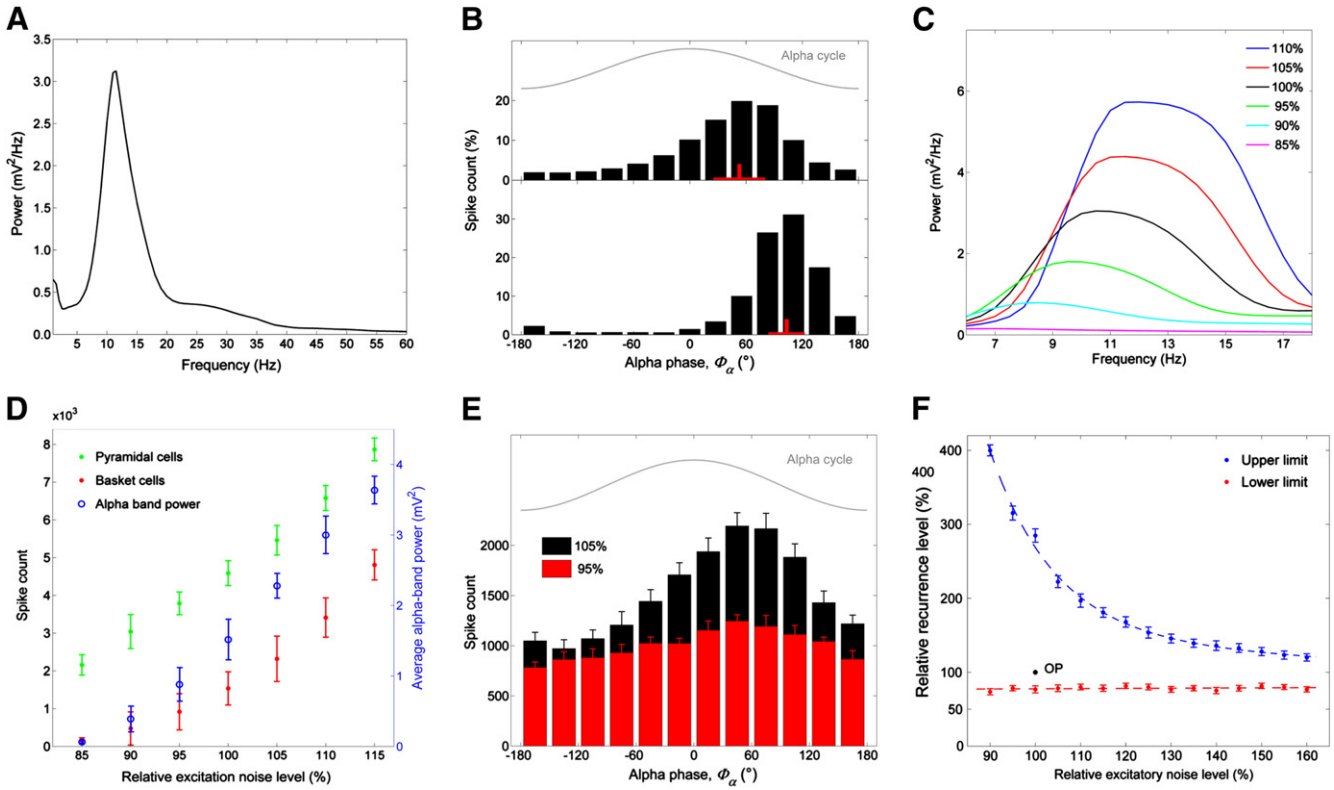

Fig. 3. Each single-area network exhibits pronounced alpha-band (10–15 Hz) oscillations that are positively correlated with noisy excitation. A: Average power spectrum of mean LFP signals in weak stimulus detection trials with slowly fluctuating noisy excitation levels (see Fig. 5). B: Phase distribution of spiking on the alpha cycle for pyramidal (top) and basket (bottom) cells. The mean phase with standard deviation is marked in red. C: Alpha power and frequency as a function of noisy excitation in the network, which is specified as a percentage of the nominal reference value. D: Correlated increase in pyramidal (green) and basket (red) cell firing with rising noisy excitation contributes to the increase in alpha power (blue). The mean spike count values and their standard deviations, shown as error bars, were estimated for all pyramidal and basket cells within one hypercolumn over 100-s period. The alpha-band power statistics were obtained in the same configuration. E: Distribution of alpha phases of spikes fired by pyramidal cells. The spike-field coupling in the alpha band is stronger for higher noisy excitation conductance (black bars for 105% and red bars for 95% of the nominal noisy excitation; PLV values were 0.22 and 0.09, respectively). The error bars describe the standard deviation of the mean number of spikes produced in the entire network and estimated for each alpha phase bin over ten 100-s trials run independently for the two noisy excitation levels. F: The range (the upper limit in blue and the lower limit in red) of recurrent pyramidal-to-pyramidal connection strengths guaranteeing bistability for different levels of noisy excitation. Both recurrent excitation and noisy excitation are given as percentages of the reference values in the nominal network's setup (the network's operating point marked as OP). The error bars correspond to the standard deviations of the pooled mean value estimates obtained from ten 100-s trials.

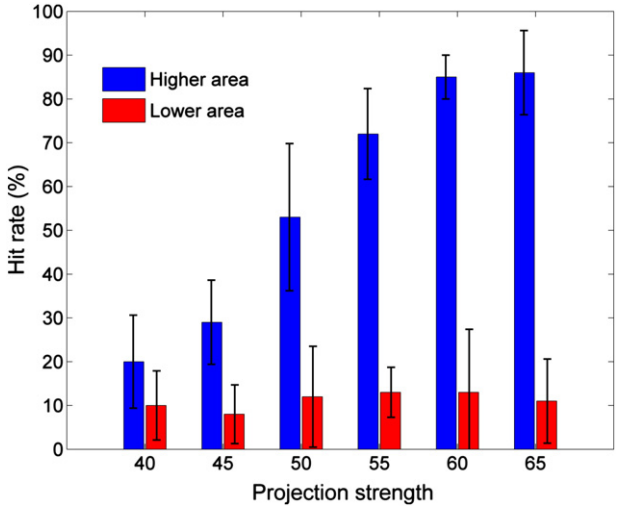

Fig. 4. The dependence of the stimulus detection rate (hit rate) in the higher associative area (blue bars) on the strength of projection from the lower sensory area (given in % of the local connection strengths). For comparison, the hit rate was also evaluated for the lower area (red bars). The error bars illustrate the standard deviation of the mean hit rate over 1000 stimulations in ten 100-s trials (derived from binomial distribution).

controlled firing rates within the system and also amplified the amplitude of the imposed ISF.

We then used 100-s simulation trials each with 100 weak stimuli (Methods section) presented once per second and examined correlation of their detection rate with the ISF phase. Unlike in the lower-order network where detection rate was not clearly ISF-phase dependent, we observed a strong correlation between detection rate and ISF phase (linear–circular correlation coefficient of 0.86, $P < 0.05$ for binned phase) in the associative network (top panel in Fig. 5B). Hit rate was maximal during periods of high noisy excitation associated with slightly elevated firing rates, increased currents and reduced average membrane potentials (here serving as LFPs).

In order to understand these detection rate modulations we investigated a wide range of noisy excitation levels in trials with stationary noise, i.e. without imposed ISFs (Methods section). Although hit rate was close to linearly related to alpha power in the range of noisy excitation where the ISFs were produced, i.e. 90–110% of the baseline level, consistently with the ISF phase modulatory effect observed in Fig. 5B, as noisy excitation was increased further hit rate displayed a strong decreasing trend (Fig. 6A). Over this wider range of alpha power, detection rate displayed inverse U-shape dependence. Some experimental studies report similar inverted U-shape behavior (Linkenkaer-Hansen et al., 2004; Rajagovianan and Ding, 2010). We could have reproduced this effect in our simulations within the

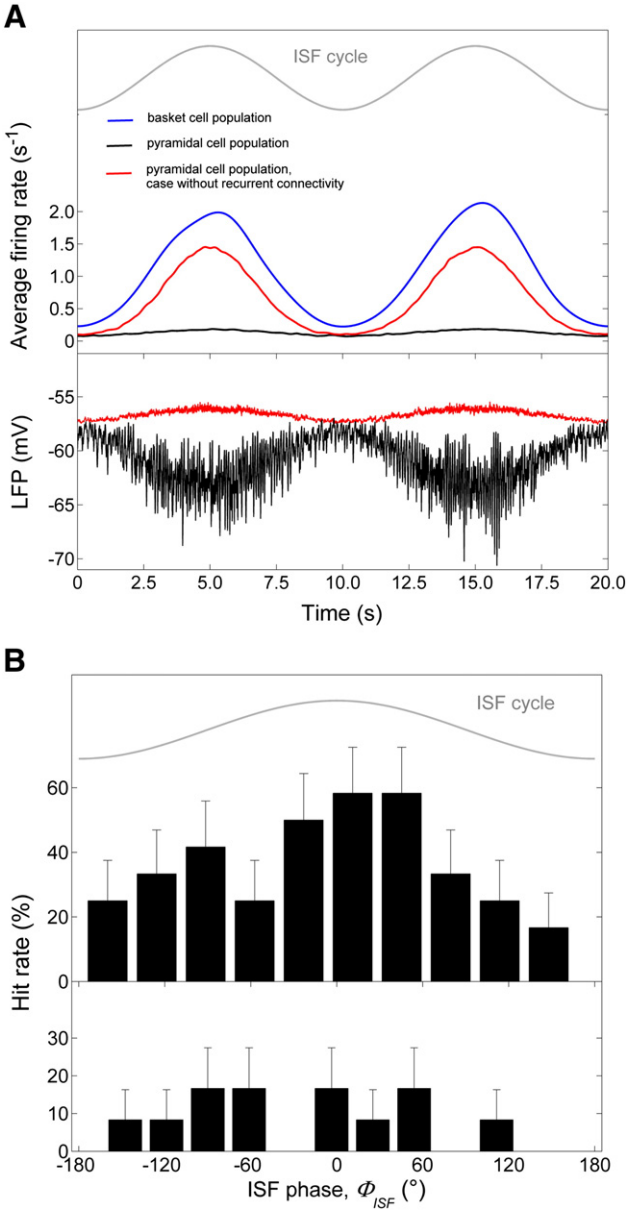

Fig. 5. ISF modulates hit rate and the amplitudes of 1–40 Hz oscillations in the higher area A: The effects of the fluctuation in noisy excitation (10% modulation by a sine wave with period of 0.1 Hz) on the network with (black) and without (red) recurrent connectivity during 20 s of simulation. ISF wave is illustrated for reference in gray, firing rate modulation in the network is shown in the top panel and the single-trial LFP from the higher area in the bottom panel. For the case with recurrent connections present we also show the firing rate modulations in the basket cell population (blue). B: The phase of the slow fluctuation (conceptual reference in gray) modulates more strongly the hit rate of weak stimuli detected in the higher area (top panel; linear–circular correlation for binned phase, $r = 0.86$, $P < 0.05$) than that in the lower area (bottom panel; $r = 0.22$, $P < 0.1$). The average hit rate was pooled over all stimulations applied to the network within given ISF phase bins in ten 100-s trials. The error bars express the standard deviation and are derived from binomial distribution.

range of ISF modulation using a small baseline shift towards higher noisy excitation that includes the level corresponding to the hit rate peak. This would have resulted in peak detection rate for intermittent rather than maximal alpha levels and thus a phase shift of the ISF phase dependence.

In the attempt to gain more insight into the modulatory effect of alpha power/excitatory noise level on stimulus detection rate, we studied the responses of individual hypercolumns in a reduced network devoid of global excitatory recurrent connections. This network operated with fixed levels of excitatory noise over the course of a single trial. Weak stimuli in the form of small EPSPs were applied to all layer 2/3 pyramidal cells within one arbitrary minicolumn in each hypercolumn in the lower patch. Without long-range recurrent connections storing attractors in the network the responses of stimulated minicolumns, quantified by the average number of spikes produced within a 400-ms window, were low and independent of noisy excitation levels (points on the ordinate axis where the relative recurrence level is 0 in Fig. 6B). Contrary to the intact network with the recurrence at the reference level, i.e. 100%, the responses were weaker in the upper network than in the lower one (dotted versus solid lines, respectively, in Fig. 6B). By gradually increasing the conductance of the long-range recurrent connections, we observed a sharp transition in the response strength (Fig. 6B) around the level of conductance where stable attractors could be activated, coinciding with the lower limit of the bistable regime (line plotted in red in Fig. 3F). However, it was rather dependence of the upper limit of the bistable regime on excitatory noise that revealed insights into the observed hit rate modulation. The exponential decrease of the upper limit with increasing excitatory noise in Fig. 3F implies that the operating point of the network with fixed recurrent connections approached the border at which attractors spontaneously activated. Even though the response of the isolated minicolumns did not grow with the noisy excitation, a smaller deviation from the ground state dynamics was needed to allow the network to settle into the stimulated attractor. This line of reasoning also explains the effect of decreasing hit rate at even higher levels of alpha-band power shown in Fig. 6A (and hence also at higher noisy excitation as evident from Fig. 3D). Namely, in this regime the change in the upper limit of the bistable range with increased noisy excitation flattens out while the signal-to-noise ratio upon stimulation, i.e. the fluctuation from the ground state quantified as the ratio of the number of spikes generated in the stimulated population and those produced in the background populations, continues to drop linearly (linear correlation, $r^2 = 0.98$, $P < 0.01$ for both patches), as shown in Fig. 6C.

We used detection latency as a second measure of the network's "psychophysical" performance. We defined it as the time from the stimulus presentation to the correct identification of the corresponding pattern in the associative network (Methods section), which would parallel the reaction time in human psychophysics. By varying the level of noisy excitation between runs, yet keeping it fixed during individual simulations, we observed a linear decrease in detection latency (Fig. 6D) with rising pre-stimulus alpha power (Bollimunta et al., 2008; Linkenkaer-Hansen et al., 2004; Mo et al., 2011; Zhang et al., 2008) and peak alpha frequency (Klimesch, 1999). Within the range of noisy excitation amplitudes that led to alpha frequencies of 8–12 Hz (the same 10% range as used for ISF, marked with gray in Fig. 6D), detection latency dropped by ~10% in approximate quantitative agreement with the experimental evidence (Linkenkaer-Hansen et al., 2004). Combined with previous results, it predicted a strong correlation between ISF phase and reaction times. A phase modulation of reaction times could indeed be observed in the ISF simulations (Fig. 7). To the best of our knowledge, this effect has not yet been investigated experimentally.

ISFs modulate power of 1–40 Hz oscillations

Single trial LFP data, demonstrated in Fig. 5A (black line in the bottom panel), suggested that the amplitudes of 1–40 Hz oscillations were also correlated with the ISF phase, as observed in experimental data (Monto et al., 2008; Nir et al., 2008; Vanhatalo et al., 2004). As shown in Fig. 8, we found similar phase-amplitude coupling between the ISF and delta/theta (1–5 Hz), alpha (8–15 Hz), upper beta (22–28 Hz) as well as gamma (30–40 Hz) rhythms while the network performed the detection task (for a direct comparison between the model and experimental results compare Fig. 8 with Fig. 4C in Monto et al., 2008). The strength of this modulation was quantified

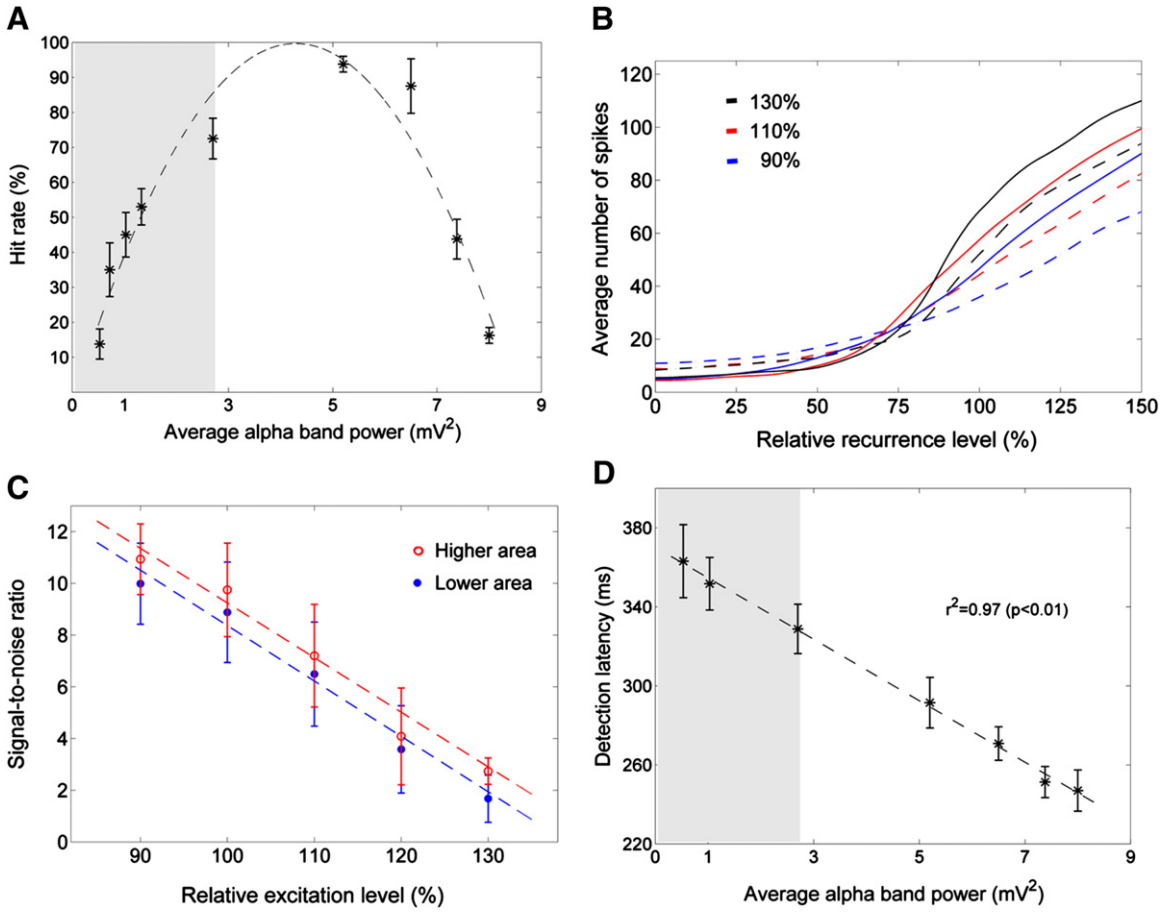

Fig. 6. Hit rate and detection latency in the associative area in relation to noisy excitation. A: Hit rate displays U-shaped dependence on pre-stimulus alpha power. The area marked in gray corresponds to the range of ISF modulation in the two-network model. The mean values and the standard deviations (shown as error bars) of the hit rate were estimated from 1000 stimulations in a total of ten 100-s trials run independently for each point shown in the figure (see Methods section). B: The number of evoked spikes in a single minicolumn of a two-area fully-sized network (9 hypercolumns) within a 400-ms time window following weak stimulation in the upper (solid lines) and lower (dashed lines) area as a function of global recurrent excitation for three noisy excitation levels: 130% in black, 110% in red and 90% in blue (100% denotes the default nominal value for both excitation sources). The results were averaged over ten 100-s trials with 100 stimulations each, run independently for each data point. Error bars are omitted for the clarity of presentation. C: The signal to-noise ratio, defined as the number of spikes generated in the stimulated population (minicolumn) relative to those produced in the background populations (remaining 48 minicolumns per hypercolumn), is plotted as a function of noisy excitation. A linear relationship can be observed in both areas (linear correlation, $r^2 = 0.98$, $P < 0.01$ for upper and lower area). The results were averaged as in B and the standard deviation of the mean is depicted as error bars. D: Detection latencies, measured in the associative area, linearly decrease with pre-stimulus alpha power ($r^2 = 0.97$, $P < 0.01$). The range corresponding to the size of ISF modulation is marked in gray. The mean values and the standard deviations of the latencies were estimated as in A and B from 1000 stimulations in a total of ten 100-s trials.

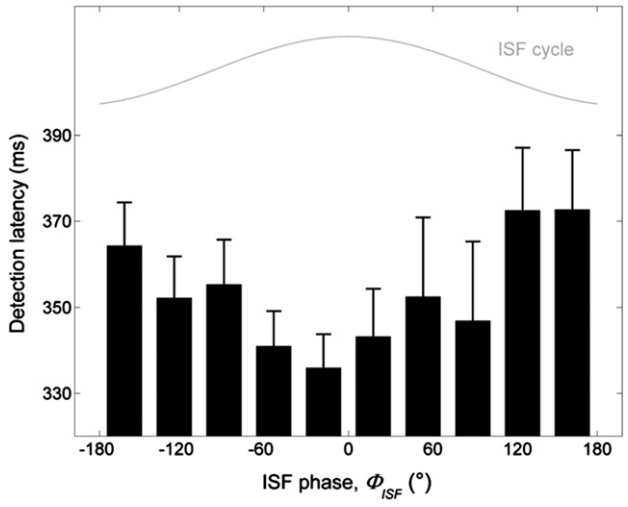

Fig. 7. Detection latency modulation by the ISF phase. The mean latency values and their standard errors were estimated from ten 100-s trials with the total of 100 stimulations applied in each phase bin (10 phase bins correspond to 10 stimulation per ISF cycle; since not all stimuli were detected the number of samples per bin varied).

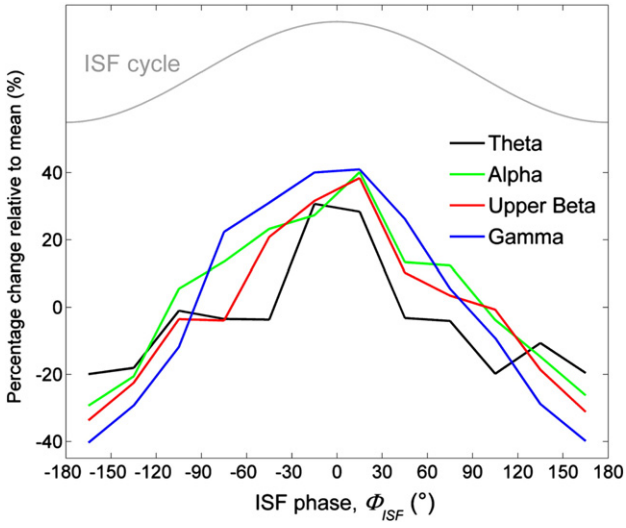

Fig. 8. Modulatory effect of ISF phase on 1–40 Hz oscillations in the higher area. The figure depicts percentage change of the average power of theta to gamma oscillations in the intervals corresponding to the binned ISF phases with respect to the overall mean (over all the phase bins). These percentage changes were averaged over 10 trials.

using within-trial PLV_{PAC} and ESC (Methods section; Bruns and Eckhorn, 2004; Vanhatalo et al., 2004) between the ISF and the other rhythms. The trial-average PLV_{PAC} estimates (mean ± std.dev.) were as follows: 0.95 ± 0.03 for gamma, 0.86 ± 0.05 for upper beta, 0.89 ± 0.03 for alpha and 0.49 ± 0.09 for theta oscillations. The corresponding ESC estimates were: −0.72 ± 0.07, −0.69 ± 0.09, −0.73 ± 0.08 and −0.45 ± 0.11, respectively. This modulation of oscillatory power explained how firing rates could be elevated during ISF troughs even though average membrane potentials were suppressed.

The origin of the phase–amplitude modulation phenomenon was two-fold. First, for the rhythms directly dependent on excitatory–inhibitory feedback loop (alpha, beta, gamma) as well as the delta/theta oscillations reflecting competition in the network, the power correlated with noisy excitation levels (but not necessarily recurrent excitation). Second, the hit rate dependence on the ISF phase constituted another factor contributing to the ISF modulation of the oscillatory power since it had a direct effect on the relative time the network spent in the ground and active attractor states. These two modulatory factors were however of a competitive nature in the case of alpha oscillations: as alpha power increased, so did the detection rate, which in turn had a negative effect on the amount of time the network spent generating this rhythm, i.e. in the ground state. Altogether, the average alpha-band power was maximum at the ISF troughs (peaks of noisy excitation), suggesting the relatively greater significance of the first factor.

Robustness of ISF modulatory effects for an alternative form of noise fluctuations

To link the present simulations with studies suggesting other mechanisms for ISF generation such as switches between global attractor states, or structured fluctuations towards such states, seen as the increased activity in a sub-group of cortical areas (; Deco and Jirsa, 2012; Deco et al., 2009; Ghosh et al., 2008; Honey et al., 2007), we generated an ISF component by imposing relatively fast switching between long-lasting states associated with lower and higher rates of noisy excitation inputs (Methods section). In this alternative setting, we then examined the nature of ISF modulatory effects and found that they remained conceptually consistent with our previous findings. We observed a bimodal instead of sinusoidal-like distribution of hit rates (Fig. 9A, dark bars in top panel) and amplitudes of 1–40 Hz oscillations (Fig. 9B). Both mechanisms thus gave rise to the same phenomena at the systems level (compare Figs. 5B and 8 with Figs. 9A,B).

In order to demonstrate that the results did not rely on having hypercolumns with strictly defined borders, we used a model with continuous hypercolumns in which the feedback inhibition implementing competition between minicolumns depended solely on their relative distance (Methods section). In this version the same attractor patterns were stored but hypercolumns emerged dynamically in the network upon the activation of a pattern: when a minicolumn became active the 48 closest surrounding minicolumns were suppressed. In consequence, the local network constituted by 49 minicolumns and the adjacent basket cells manifested similar dynamics to that of a hypercolumn in the original model except that the borders of the emerging local networks shifted depending on which minicolumns were activated. Despite this modification in the model, the oscillatory power and hit rate modulation by ISF phase was preserved (compare Figs. 9A,B with Figs. 9C,D).

Discussion

We presented an attractor network model that displayed a slow component akin to ISFs in the synthesized LFP due to imposed low-rate changes in the amplitude of fast noisy excitation. The functional and dynamical impact of these ISFs were consistent with key experimental findings: the ISF modulated amplitudes of 1–40 Hz oscillations (Monto et al., 2008; Nir et al., 2008; Vanhatalo et al., 2004), firing rates (Albrecht and Gabriel, 1994; Allers et al., 2002; Lörincz et al., 2009; Nir et al., 2008; Ruskin et al., 2003; Werner and Mountcastle, 1963), as well as psychophysical hit rates (Monto et al., 2008) and reaction times (Linkenkaer-Hansen et al., 2004) in a simulated stimulus detection task. We also found that detection latency was correlated with both peak alpha frequency (Klimesch, 1999) and alpha power (Linkenkaer-Hansen et al., 2004; Mo et al., 2011). Hence, our model concurrently reproduced a wide range of electrophysiological and behavioral phenomena, and may thus yield insight into the underlying neuronal mechanisms and generate novel experimentally testable hypotheses.

Model simplifications

Although the model produced results compatible with experimental findings observed at different levels of brain organization, it is still simplified in several aspects. We employed a biophysically detailed attractor network (Lundqvist et al., 2006) operating in a bistable regime (Djurfeldt et al., 2008; Lundqvist et al., 2010) with alpha-like oscillations in the ground state and nested theta–gamma oscillations in the coding state. Identical copies of this network were used to represent both the stimulated lower-order and associative network. Since the rate of stimulus-triggered attractor activations was low in the lower-order network, our results did not impinge on its capacity to store attractor patterns. Therefore the lower-order part of the model could have been implemented in several other ways, for instance as a network retaining lower-order information (Lee et al., 2002). Each cortical patch was significantly reduced in size relative to a cortical area, but the model had previously been scaled up to the size of a full mouse cortex with the dynamics retained (Djurfeldt et al., 2008). Furthermore, we did not include layer 5 in our model as we hypothesized that attractor dynamics should be most pronounced in superficial layers of associative cortex (Lundqvist et al., 2011). Dense excitatory recurrent connections supporting attractor dynamics have indeed been found in abundance in layer 2/3 (Binzegger et al., 2009), where the main driving force of sustained activity in the cortex has been localized (Binzegger et al., 2009; Weiler et al., 2008). Accordingly, we attribute the origin of theta and gamma rhythms, i.e. correlates of active retrieval in our model, to layer 2/3 (Chrobak and Buszaki, 1998; Fries et al., 2008).

The level of biological detail in the model implementation could have likely been either increased (e.g., by adding a second type of inhibitory neuron population responsible for theta generation) or decreased (e.g., by using point neuron models) without strong qualitative implications for the reported results (Krishnamurthy et al., 2012). The key features of the model stemmed from a few key facts. First, structured horizontal excitatory connections (Muir et al., 2011) stored global activation patterns coding for distinct input. Second, strong feedback inhibition underlay the stability of a non-coding ground state, characterized by global unstructured activity (Amit and Brunel, 1997). Third, the network's hypercolumnar structure, resulting from the limited spatial extent of such feedback inhibition (Yuan et al., 2011), stabilized the coding attractors in the lower ranges of excitation (Lundqvist et al., 2010). These latter two factors allowed us to vary noisy excitation over a wide range, hence affecting quantitative measures such as detection rate and alpha-band power, while qualitatively remaining within the same, bistable, regime. The strict hypercolumnar modular structure was indeed also a simplification, where feedback inhibition was restricted to target only minicolumns inside a predefined hypercolumn. This is likely not the case in most cortical areas where individual hypercolumnar modules are often hard to discern by histology. This limitation however could be removed with the core dynamics retained. In this setup, feedback inhibition was set by spatial distance

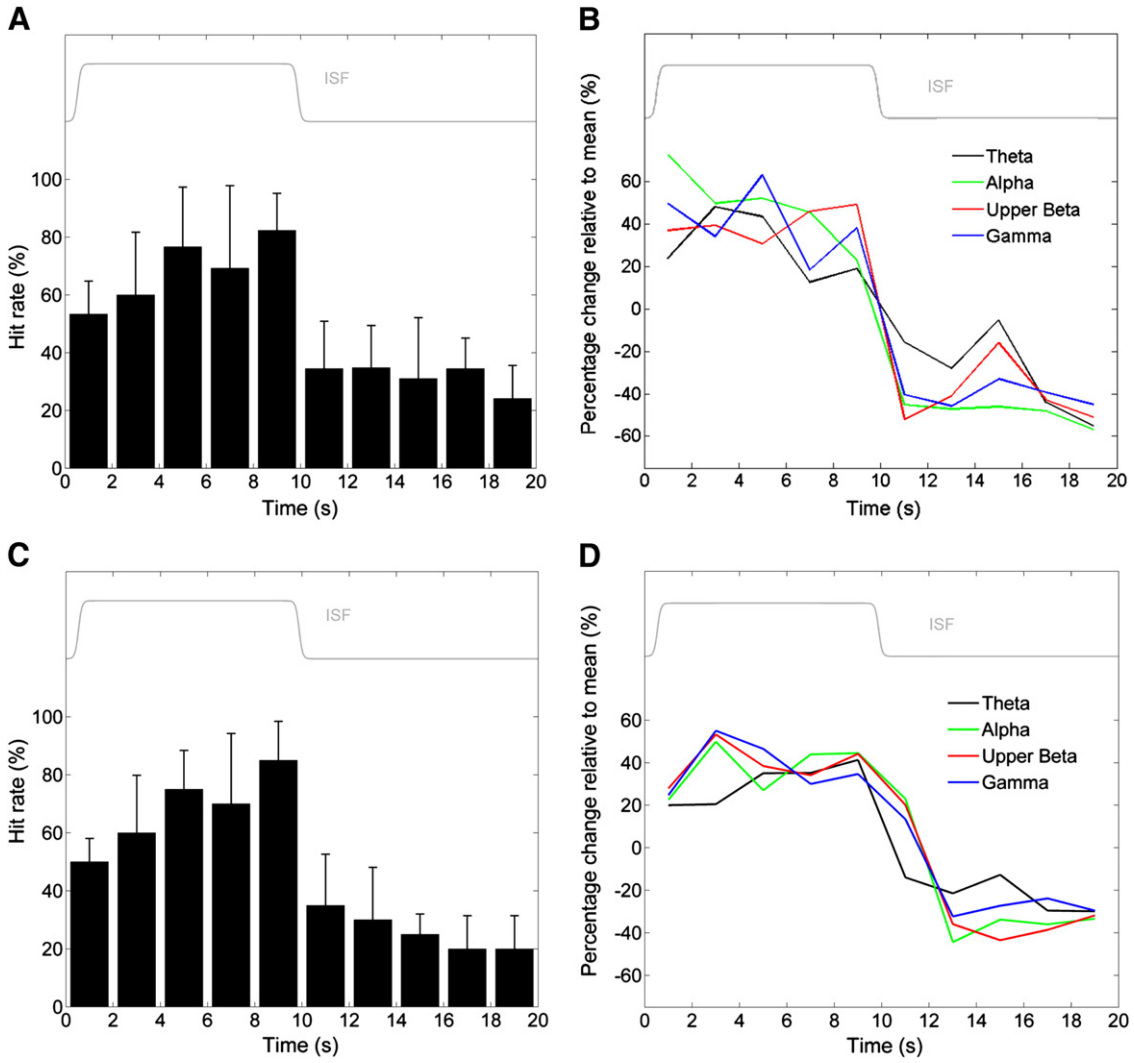

Fig. 9. ISFs imposed by a low-rate pulse modulation of firing rates of the noisy excitation. A: Hit rate modulation in the associative network by the ISF with bimodally distributed power (the reference pulse cycle is shown in gray). The average hit rate was pooled over all stimulations applied to the network at the rate of 1 s^{-1} in ten 100-s trials. The error bars express the standard deviation and are derived from binomial distribution. B: Modulation of 1–40 Hz oscillation amplitudes by ISF (the reference pulse cycle is shown in gray). The results were averaged over ten 100-s trials. C: Same as A, but using a model with continuous hypercolumns (see Methods section). D: Same as B, but using a model with continuous hypercolumns (see Methods section).

alone (Yuan et al., 2011) and the hypercolumns were only reflected in the dynamics during the activation of an attractor pattern.

Functional networks and origin of ISFs

The findings reported here were also largely independent of the precise nature and source of fluctuations in excitation and excitability levels. In vivo, both single cell- and network-level effects are likely to concurrently contribute to ISF generation (Palva and Palva, 2012). We therefore used noise level manipulations, the hypothesized output of this interaction, as a starting point to study the function of ISFs in a manner independent on assumptions about mechanisms generating the ISFs per se. We imposed the ISFs on the network by means of either a sinusoidal modulation of background excitatory noise mimicking e.g. astrocytic Ca^{2+} oscillations (Lörincz et al., 2009) or by switches between two distinct frequencies in the background population activity. The latter implementation was motivated by several previous modeling studies on the genesis of ISFs using bistable networks of a relatively large scale but with relatively low level of biological detail (Deco and Jirsa, 2012; Deco et al., 2009; Ghosh et al., 2008; Honey et al., 2007). In a multi-scale approach, our network could be submerged into such a network of networks. A spontaneous activation of a functional network would then correspond to the increased background activity in a subset of cortical areas, here simulated by increased frequency of noisy excitation. Such fast switches between two levels of noisy excitation, and thus alpha power, are also compatible with the observed bistability in alpha-band power (Freyer et al., 2009).

In agreement with the modeling studies mentioned above, experimental evidence suggests that ISFs could reflect task-dependent switches between functional connectivity networks (for review, see (Palva and Palva, 2012)) observed in resting state studies (Fransson, 2005; Greicius et al., 2003). Activation of such networks has also been observed to correlate with changes in oscillatory power (Goldman et al., 2002; Leopold et al., 2003; Mantini et al., 2007; Sadaghiani et al., 2010) and psychophysical performance (Sadaghiani et al., 2009).

Alpha oscillations and psychophysical performance

In this study, changes in alpha-band power reflected fluctuations in excitability on an infra-slow time scale. Within the range of noisy excitation where ISFs were produced, a linear relationship between hit rate and pre-stimulus alpha power was observed due to a gradual

destabilization of the ground state. Experimentally, the functional correlates of alpha oscillations are still a matter of debate (Klimesch and Sauseng, 2007; Palva and Palva, 2007; J.M. Palva et al., 2010; Pfurtscheller et al., 1996; Sadaghiani et al., 2009, 2010). Pre-stimulus alpha power in TSDTs has been shown to be both positively (Linkenkaer-Hansen et al., 2004; Zhang et al., 2008) and negatively (Hanslmayr et al., 2007) correlated with psychophysical performance. Recent studies on the origins of alpha oscillations have shed more light on these seemingly conflicting findings (Bollimunta et al., 2008, 2011; Mo et al., 2011) with the laminar origin playing a central role. When the alpha generation occurred in the deeper layers of low-level sensory cortices, power was positively correlated with reaction times in a visual task. Higher in the processing stream, in the inferior temporal cortex, however, alpha was generated in the superficial layers and correlated negatively with reaction times (Bollimunta et al., 2008). Then, increased pre-stimulus alpha power led to stronger stimulus evoked gamma power and elevated firing rates (Mo et al., 2011). The inferior temporal cortex findings are consistent with the behavior of our layer 2/3 network, and also with EEG recordings over parietal (Linkenkaer-Hansen et al., 2004) and prefrontal (Monto et al., 2008) areas. Importantly, stimulus induced switches from alpha to gamma oscillations, similar to those observed in our network, have been observed specifically in layer 2/3 of macaque cortex (Buffalo et al., 2011; Fries et al, 2008).

Several of our results were based on the correlation between alpha power and noisy excitatory drive of the network. Noisy excitation also had a direct effect on the number of cells participating in prestimulus firing. These dependencies, endogenously emerging from our model's intrinsic dynamics, are in line with experimental observations that increased alpha power in superficial layers is positively correlated with firing rates during attentive cognitive states (Mo et al., 2011). In contrast to earlier modeling studies of alpha oscillations (Jones et al., 2000; Karameh et al., 2006; Rotstein et al, 2005; Smerieri et al, 2010; Vieerling-Claassen et al., 2010), our network included a large number of neurons and only a small fraction of cells needed to fire each cycle to perpetuate the oscillatory regime. This fraction increased with excitatory drive, affecting the oscillation amplitude of the network. Thus, in the aforementioned studies the alpha frequency was typically determined by synaptic time constants, while in our network the 10–40 Hz oscillations were produced by the same excitatory–inhibitory feedback loop. Distinct alpha and gamma rhythmicity arose instead from having two separate functional states with inherently different levels of excitation (Lundqvist et al., 2010) dynamically controlling the frequency (Brunel and Wang, 2003).

Overall, these alternative modeling approaches suggest that individual and age-related differences in alpha frequency (Klimesch, 1999) reflect variability in either synaptic time constants or in levels of excitation. The latter interpretation would predict stronger dynamical fluctuations in the peak alpha frequency, which could be tested experimentally with fluctuation analyses (Linkenkaer-Hansen et al., 2001) and investigations of alpha frequency in full-band EEG recordings exhibiting ISFs during TSDT experiments (e.g., as in Monto et al., 2008). An effect of ISF phase not only on alpha power but also on its dominant frequency should be expected. This prediction is indirectly supported by reported correlations between alpha frequency and reaction times (Klimesch, 1999), and between reaction times and alpha power (Mo et al., 2011). In addition, our results predict a modulatory effect of ISFs on reaction times.

Our model does not account for layer 5 cortico-cortical (Silva et al., 1991) or for thalamo-cortical interaction in the generation of alpha oscillations (Hughes and Crunelli, 2005; Robinson et al., 2001) that exhibit an inverse relationship with cortical excitability (Bollimunta et al., 2008; Hanslmayr et al., 2007). This should be incorporated in a more comprehensive network model including layers 5 and 6 (Jones et al., 2000, 2007, 2009; Karameh et al., 2006), where the combined impact of top-down and feedforward alpha on stimulus detection could be studied (Beck and Kastner, 2009; Jones et al., 2007). Our results still yield insights into the dynamics and functional implications of alpha and theta/gamma oscillations generated in layer 2/3, modulated by top-down feedback system. The superficial alpha could reflect top-down prefrontal attentional drive (Beck and Kastner, 2009; Mo et al., 2011), which in the model could bias some attractors (Deco and Thiele, 2009) so that the spiking during alpha oscillations contained task-relevant information (Palva and Palva, 2007).

ISFs and 1–40 Hz oscillations

The two distinct functional and dynamical states of the network produced either alpha (non-coding ground state) or nested theta and gamma rhythms (attractor retrieval) (Djurfeldt et al., 2008; Lundqvist et al., 2010, 2011, 2012). Specifically, a theta wave was produced for each activation of an attractor, and was a carrier for nested gamma oscillations (Lundqvist et al., 2011, 2012). Such nested oscillations are believed to be connected to active processing in vivo (Canolty et al, 2006; Kendrick et al., 2011; Lakatos et al., 2005; J.M. Palva et al., 2005). The rhythms within 1–40 Hz band have been demonstrated experimentally to be co-modulated by ISF phase (Monto et al., 2008; Nir et al., 2008), as was faithfully reproduced by the model. Specifically, hit rate dependence on noisy excitation gave rise to modulation of theta- and gamma-band power. The model thus predicts that this effect is weaker when few or no stimuli are presented. For the alpha rhythm, however, the opposite is expected in such cases.

Conclusions

We have shown that a biophysically detailed model of an attractor network hierarchy provides a promising framework for reproducing and understanding the correlations among ISFs, fast neuronal oscillations, and psychophysical performance in resting state and during task performance. In consequence, based on modeling insights, we make several predictions for experimental work. Finally, the results provide further validation for the attractor hypothesis of cortical function and support the idea that superficial layers for cortex have functional characteristics compatible with those of attractor memory networks.

Acknowledgments

This work was partly supported by grants from the Swedish Science Council (Vetenskapsrådet, VR-621-2009-3807), the VINNOVA (Swedish Governmental Agency for Innovation Systems), the Swedish Foundation for Strategic Research (through the Stockholm Brain Institute), and from the European Union (BrainScales, EU-FP7-FET-269921).

Conflict of interest

The authors declare that they have no conflict of interest in the work described in this study, financial or otherwise.

References

Aladjalova, N.A., 1957. Infra-slow rhythmic oscillations of the steady potential of the cerebral cortex. Nature 179, 957–959.
Albrecht, D., Gabriel, S., 1994. Very slow oscillations of activity in geniculate neurones of urethane-anaesthetized rats. Neuroreport 5, 1909–1912.
Allers, K.A., Ruskin, D.N., Bergstrom, D.A., Freeman, L.E., Ghazi, L.J., Tierney, P.L., Walters, J.R., 2002. Multisecond periodicities in basal ganglia firing rates correlate with theta bursts in transcortical and hippocampal EEG. J. Neurophysiol. 87, 1118–1122.
Amit, D.J., Brunel, N., 1997. Model of global spontaneous activity and local structured activity during delay periods in cerebral cortex. Cereb. Cortex 7, 237–252.
Beck, D.B., Kastner, S., 2009. Top-down and bottom-up mechanisms in biasing competition in human brain. Vision Res. 49, 1154–1165.

Binzegger, T., Douglas, R.J., Martin, K.A.C., 2009. Topology and dynamics of the canonical circuit of cat V1. Neural Netw. 22, 1071–1078.

Biswal, B., Yetkin, F.Z., Haughton, V.M., Hyde, J.S., 1995. Functional connectivity in the motor cortex of resting human brain using echo-planar MRI. Magn. Reson. Med. 34, 537–541.

Bollimunta, A., Chen, Y., Schroeder, C.E., Ding, M., 2008. Neural mechanisms of cortical alpha oscillations in awake-behaving macaques. J. Neurosci. 28, 9976–9988.

Bollimunta, A., Mo, J., Schroeder, C.E., Ding, M., 2011. Neuronal mechanisms and attentional modulation of corticothalamic alpha oscillations. J. Neurosci. 31, 4935–4943.

Brookes, M.J., Woolrich, M., Luckhoo, H., Price, D., Hale, J.R., Stephenson, M.C., Barnes, G.R., Smith, S.M., Morris, P.G., 2011. Investigating the electrophysiological basis of resting state networks using magnetoencephalography. Proc. Natl. Acad. Sci. 108, 16783–16788.

Brunel, N., Hakim, V., 1999. Fast global oscillations in networks of integrate-and-fire neurons with low firing rates. Neural Comput. 11, 1621–1671.

Brunel, N., Wang, X.J., 2003. What determines the frequency of fast network oscillations with irregular neural discharges? I. Synaptic dynamics and excitation–inhibition balance. J. Neurophysiol. 90, 415–430.

Bruns, A., Eckhorn, R., 2004. Task-related coupling from high- to low-frequency signals among visual cortical areas in human subdural recordings. Int. J. Psychophysiol. 51, 97–116.

Buffalo, A.E., Fries, P., Landman, R., Buschman, T.J., Desimone, R., 2011. Laminar differences in gamma and alpha coherence in the ventral stream. Proc. Natl. Acad. Sci. 108, 11262–11267.

Canolty, R.T., Edwards, E., Dalai, S.S., Soltani, M., Nagarajan, S.S., Kirsch, H.E., Berger, M.S., Barbaro, N.M., Knight, R.T., 2006. High gamma power is phase-locked to theta oscillations in human neocortex. Science 313, 1626–1628.

Carnevale, N.T., Hines, M.L., 2006. The Neuron Book. Cambridge University Press.

Chrobak, J.J., Buszaki, G., 1998. Gamma oscillations in the entorhinal cortex of the freely behaving rat. J. Neurosci. 18, 388–398.

Deco, G., Jirsa, V., 2012. Ongoing cortical activity at rest: criticality, multistability, and ghost attractors. J. Neurosci. 32, 3366–3375.

Deco, G., Thiele, A., 2009. Attention — oscillations and neuropharmacology. Eur. J. Neurosci. 30, 347–354.

Deco, G., Jirsa, V., McIntosh, A.R., Sporns, O., Kötter, R., 2009. Key role of coupling, delay, and noise in resting brain fluctuations. Proc. Natl. Acad. Sci. 106, 10302–10307.

Dehaene, S., Changeux, J.-P., 2011. Experimental and theoretical approaches to conscious processing. Neuron 70, 200–227.

Dehaene, S., Changeux, J.-P., Naccache, L., Saccur, J., Sergent, C., 2006. Conscious, preconscious, and subliminal processing: a testable taxonomy. TICS 10, 204–211.

Djurfeldt, M., Lundqvist, M., Johansson, C., Rehn, M., Ekeberg, Ö., Lansner, A., 2008. Brain-scale simulation of the neocortex on the IBM Blue Gene/L supercomputer. IBM J. Res. Dev. 52, 31–41.

Fisher, N.I., 1995. Statistical Analysis of Circular Data. Cambridge UP, Cambridge, UK.

Fransén, E., Lansner, A., 1995. Low spiking rates in a population of mutually exciting pyramidal cells. Network 6, 271–288.

Fransson, P., 2005. Spontaneous low-frequency BOLD signal fluctuations: an fMRI investigation of the resting-state default mode of brain function hypothesis. Hum. Brain Mapp. 26, 15–29.

Freyer, F., Aquino, K., Robinson, P.A., Ritter, P., Breakspear, M., 2009. Bistability and non-Gaussian fluctuations in spontaneous cortical activity. J. Neurosci. 29, 8512–8524.

Fries, P., Womelsdorf, T., Oostenveld, R., Desimone, R., 2008. The effects of visual stimulation and selective visual attention on rhythmic neuronal synchronization in macaque area V4. J. Neurosci. 28, 4823–4835.

Ghosh, A., Rho, Y., McIntosh, A.R., Kötter, R., Jirsa, V.K., 2008. Noise during rest enables the exploration of the brain's dynamic repertoire. PLoS Comput. Biol. 4, e1000196. http://dx.doi.org/10.1371/journal.pcbi.1000196.

Girard, P., Hupé, J.M., Bullier, J., 2001. Feedforward and feedback connections between areas V1 and V2 of the monkey have similar rapid conduction velocities. J. Neurophysiol. 85, 1328–1331.

Goldman, R.I., Stern, J.M., Engel Jr., J., Cohen, M.S., 2002. Simultaneous EEG and fMRI of the alpha rhythm. Neuroreport 13, 2487–2492.

Greicius, M.D., Krasnow, B., Reiss, A.L., Menon, V., 2003. Functional connectivity in the resting brain: a network analysis of the default mode hypothesis. Proc. Natl. Acad. Sci. 100, 253–258.

Hanslmayr, S., Aslan, A., Staudigl, T., Klimesch, W., Herrmann, C.S., Bäuml, K.-H., 2007. Prestimulus oscillations predict visual perception performance between and within subjects. Neuroimage 37, 1465–1473.

Honey, J.C., Kötter, R., Breakespear, M., Sporns, O., 2007. Network structure of cerebral cortex shapes functional connectivity on multiple time scales. Proc. Natl. Acad. Sci. 104, 10240–10245.

Hughes, S.W., Crunelli, V., 2005. Thalamic mechanisms of EEG alpha rhythms and their pathological implications. Neuroscientist 11, 357–372.

Hughes, S.W., Lorincz, M.L., Parri, H.R., Crunelli, V., 2011. Infraslow (<0.1 Hz) oscillations in thalamic relay nuclei basic mechanisms and significance to health and disease states. Prog. Brain Res. 193, 145–162.

Jones, S.R., Pinto, D.J., Kaper, T.J., Kopell, N., 2000. Alpha-frequency rhythms desynchronize over long cortical distances: a modeling study. J. Comput. Neurosci. 27, 271–291.

Jones, S.R., Pritchett, D.L., Stufflebeam, S.M., Hamalainen, M., Moore, C.I., 2007. Neural correlates of tactile detection: a combined MEG and biophysically based computational modeling study. J. Neurosci. 27, 10751–10764.

Jones, S.R., Pritchett, D.L., Sikora, M.A., Stufflebeam, S.M., Hämäläinen, M., Moore, C.I., 2009. Quantitative analysis and biophysically realistic neural modeling of the MEG Mu rhythm: rhythmogenesis and modulation of sensory-evoked responses. J. Neurophysiol. 102, 3554–3572.

Kampa, B.M., Letzkus, J.J., Stuart, G.J., 2006. Cortical feed-forward networks for binding different streams of sensory information. Nat. Neurosci. 9, 1472–1473.

Karameh, F.N., Dahleh, M.A., Brown, E.N., Massaquoi, S.G., 2006. Modeling the contribution of lamina 5 neuronal and network dynamics to low frequency EEG phenomena. Biol. Cybern. 95, 289–310.

Kendrick, K.M., Zhan, Y., Fisher, H., Nicol, A.U., Zhang, X., Feng, J., 2011. Learning alters the theta amplitude, theta–gamma coupling and neural synchronization in inferotemporal cortex. BMC Neurosci. 12, 55.

Klausberger, T., Somogyi, P., 2008. Neuronal diversity and temporal dynamics: the unity of hippocampal circuit operations. Science 321, 53–57.

Klimesch, W., 1999. EEG alpha and theta oscillations reflect cognitive and memory performance: a review and analysis. Brain Res. Rev. 29, 169–195.

Klimesch, W., Sauseng, P., 2007. EEG alpha oscillations: the inhibition–timing hypothesis. Brain Res. Rev. 53, 63–88.

Krishnamurthy, P., Silberberg, G., Lansner, A., 2012. A cortical attractor network with Martinotti cells driven by facilitating synapses. PLoS One 7, e30752. http://dx.doi.org/10.1371/journal.pone.0030752.

Lachaux, J.P., Rodriguez, E., Martinerie, J., Varela, F.J., 1999. Measuring phase synchrony in brain signals. Hum. Brain Mapp. 8, 194–208.

Lakatos, P., Shah, A.S., Knuth, K.H., Ulbert, I., Karmos, G., Schroeder, C.E., 2005. An oscillatory hierarchy controlling neuronal excitability and stimulus processing in the auditory cortex. J. Neurophysiol. 94, 1904–1911.

Lee, T.S., Yang, C.F., Romero, R.D., Mumford, D., 2002. Neural activity in early visual cortex reflects behavioral experience and higher-order perceptual saliency. Nat. Neurosci. 5, 589–597.

Leopold, D.A., Murayama, Y., Logothetis, N.K., 2003. Very slow activity fluctuations in monkey visual cortex: implications for functional brain imaging. Cereb. Cortex 13, 422–433.

Linkenkaer-Hansen, K., Nikouline, V.V., Palva, J.M., Ilmoniemi, R.J., 2001. Long-range temporal correlations and scaling behavior in human brain oscillations. J. Neurosci. 21, 1370–1371.

Linkenkaer-Hansen, K., Nikulin, V.V., Palva, S., Ilmoniemi, R.J., Palva, M., 2004. Prestimulus oscillations enhance psychophysical performance in humans. J. Neurosci. 24, 10186–10190.

Lörincz, M.L., Geall, F., Bao, Y., Crunelli, V., Huges, S.W., 2009. ATP-dependent infra-slow (<0.2 Hz) oscillations in thalamic networks. PLoS One 4, e4447.

Lundqvist, M., Rehn, M., Djurfeldt, M., Lansner, A., 2006. Attractor dynamics in a modular network model of neocortex. Network 17, 253–276.

Lundqvist, M., Compte, A., Lansner, A., 2010. Bistable, irregular firing and population oscillations in a modular attractor memory network. PLoS Comput. Biol. 6, e1000803. http://dx.doi.org/10.1371/journal.pcbi.1000803.

Lundqvist, M., Herman, P., Lansner, A., 2011. Theta and gamma power increases and alpha/beta power decreases with memory load in an attractor network model. J. Cogn. Neurosci. 23, 3008–3020.

Lundqvist, M., Herman, P., Lansner, A., 2012. Variability of spike firing during theta-coupled replay of memories in a simulated attractor network. Brain Res. 1434, 152–161.

Mantini, D., Perrucci, M.G., Del Gratta, C., Romani, G.L., Corbetta, M., 2007. Electrophysiological signatures of resting state networks in the human brain. Proc. Natl. Acad. Sci. 104, 13170–13175.

Mo, J., Schroeder, C.E., Ding, M., 2011. Attentional modulation of alpha oscillations in macaque inferotemporal cortex. J. Neurosci. 31, 878–882.

Monto, S., Palva, S., Voipio, J., Palva, J.M., 2008. Very slow EEG fluctuations predict the dynamics of stimulus detection and oscillation amplitudes in humans. J. Neurosci. 28, 8268–8272.

Muir, D.R., Da Costa, N.M.A., Girardin, C.C., Naaman, S., Omer, D.B., Ruesch, E., Grinvald, A., Douglas, R.J., 2011. Embedding of cortical representations by the superficial patch system. Cereb. Cortex. http://dx.doi.org/10.1093/cercor/bhq290.

Nir, Y., Mukamel, R., Dinstein, I., Privman, E., Harel, M., Fisch, L., Gelbard-Sagiv, H., Kipervasser, S., Andelman, F., Neufeld, M.Y., Kramer, U., Arieli, A., Fried, I., Malach, R., 2008. Interhemispheric correlations of slow spontaneous neuronal fluctuations revealed in human sensory cortex. Nat. Neurosci. 11, 1100–1108.

Norton, S., Jewett, R.E., 1965. Frequencies of slow potential oscillations in the cortex of cats. Electroencephalogr. Clin. Neurophysiol. 19, 377–386.

Okun, M., Naim, A., Lampl, I., 2010. The subthreshold relation between cortical local field potential and neuronal firing unveiled by intracellular recordings in awake rats. J. Neurosci. 30, 4440–4448.

Oostenveld, R., Fries, P., Maris, E., Schoffelen, J.M., 2011. FieldTrip: open source software for advanced analysis of MEG, EEG, and invasive electrophysiological data. Comput. Intell. Neurosci. http://dx.doi.org/10.1155/2011/156869.

Palva, S., Palva, J.M., 2007. New vistas for alpha-frequency band oscillations. Trends Neurosci. 30, 150–158.

Palva, J.M., Palva, S., 2012. Infra-slow fluctuations in electrophysiological recordings, blood-oxygenation-level-dependent signals, and psychophysical time series. Neuroimage 62, 2201–2211.

Palva, J.M., Palva, S., Kaila, K., 2005. Phase synchrony among neuronal oscillations in the human cortex. J. Neurosci. 25, 3962–3972.

Palva, S., Linkenkaer-Hansen, K., Näätänen, Palva J.M., 2005. Early neural correlates of conscious somatosensory perception. J. Neurosci. 25, 5248–5258.

Palva, J.M., Monto, S., Kulashekhar, S., Palva, S., 2010. Neural synchrony reveals working memory networks and predicts individual memory capacity. Proc. Natl. Acad. Sci. 107, 7580–7585.

Penttonen, M., Nurminen, N., Miettinen, R., Sirviö, J., Henze, D.A., Csicsvári, J., Buszáki, G., 1999. Ultra-slow oscillation (0.025 Hz) triggers hippocampal afterdischarges in Wistar rats. Neuroscience 94, 735–743.

Peters, A., Yilmaz, E., 1993. Neurological organization in area 17 of cat visual cortex. Cereb. Cortex 3, 49–68.

Pfurtscheller, G., Stancák, A., Neuper, C., 1996. Event-related synchronization (ERS) in the alpha band: an electrophysiological correlate of cortical idling. Int. J. Psychophysiol. 24, 39–46.
Power, J.D., Cohen, A.L., Nelson, S.M., Gagan, S.W., Barnes, K.A., Church, J.A., Vogel, A.C., Laumann, T.O., Miezen, F.M., Schlaggar, B.L., Petersen, S.E., 2011. Functional network organization of the human brain. Neuron 72, 665–678.
Rajagovianan, R., Ding, M., 2010. From prestimulus alpha oscillation to visual-evoked response: an inverted-U function and its attentional modulation. J. Cogn. Neurosci. 23, 1379–1394.
Robinson, P.A., Rennie, C.J., Wright, J.J., 1997. Propagation and stability of waves of electrical activity in the cerebral cortex. Phys. Rev. E Stat. Nonlin. Soft Matter Phys. 56, 826–840.
Robinson, P.A., Rennie, C.J., Wright, J.J., Bahramali, H., Gordon, E., Rowe, D.L., 2001. Prediction of electroencephalographic spectra from neurophysiology. Phys. Rev. E Stat. Nonlin. Soft Matter Phys. 63, 1–18.
Rotstein, H.G., Pervouchine, D.D., Acker, C.D., Gillies, M.J., White, J.A., Buhl, E.H., Whittington, M.A., Kopell, N., 2005. Slow and fast inhibition and an H-current interact to create a theta rhythm in a model of CA1 interneuron network. J. Neurophysiol. 107, 1509–1518.
Ruskin, D.N., Bergstrom, D.A., Tierney, P.L., Walters, J.R., 2003. Correlated multisecond oscillations in firing rate in the basal ganglia: modulation by dopamine and the subthalamic nucleus. Neuroscience 117, 427–438.
Sadaghiani, S., Hesselmann, G., Kleinschmidt, A., 2009. Distributed and antagonistic contributions of ongoing activity fluctuations of auditory stimulus detection. J. Neurosci. 29, 13410–13417.
Sadaghiani, S., Scheeringa, R., Lehongre, K., Morillion, B., Giraud, A.-L., Kleinschmidt, A., 2010. Intrinsic connectivity networks, alpha oscillations and tonic alertness: a simultaneous electroencephalography/functional magnetic resonance imaging study. J. Neurosci. 30, 40243–40250.
Silva, L.R., Amitai, Y., Connors, B.W., 1991. Intrinsic oscillations of neocortex generated by layer 5 pyramidal neurons. Science 251, 432–435.
Silverstein, D., Lansner, A., 2011. Is attentional blink a byproduct of neocortical attractors? Front. Comput. Neurosci. 5, 1–14.
Slepian, D., Pollak, H.O., 1961. Prolate spheroidal wave functions: Fourier analysis and uncertainty I. Bell Syst. Tech. J. 40, 43–63.
Smerieri, A., Rolls, E.T., Feng, J., 2010. Decision time, slow inhibition, and theta rhythm. J. Neurosci. 30, 14173–14181.
Thomson, D., 1982. Spectrum estimation and harmonic analysis. Proc. IEEE (70), 1055–1096.
Thomson, A.M., West, D.C., Wang, Y., Bannister, A.P., 2002. Synaptic connections and small circuits involving excitatory and inhibitory neurons in layers 2–5 of adult rat and cat neocortex: triple intracellular recordings and biocytin labelling in vitro. Cereb. Cortex 12, 936–953.
Tsodyks, M., Pawelzik, K., Markram, H., 1998. Neural networks with dynamical synapses. Neural Comput. 10, 821–835.
Ursino, M., La Cara, G., 2006. Travelling waves and EEG patterns during epileptic seizure: analysis with an integrate and fire neuron. J. Theor. Biol. 242, 171–187.
Vanhatalo, S., Palva, J.M., Holmes, M.D., Miller, J.W., Voipio, J., Kaila, K., 2004. Infraslow oscillations modulate excitability and interictal epileptic activity in the human cortex during sleep. Proc. Natl. Acad. Sci. 101, 5053–5057.
Vieerling-Claassen, D., Cardin, J.A., Moore, C.I., Jones, S.R., 2010. Computational modeling of distinct neocortical oscillations driven by cell-type selective optogenetic drive: separable resonant circuits controlled by low-threshold spiking and fast-spiking interneurons. Front. Hum. Neurosci. 4, 198.
Vinck, M., Battaglia, F.P., Womelsdorf, T., Pennartz, C., 2011. Improved measures of phase-coupling between spikes and the local field potential. J. Comput. Neurosci. http://dx.doi.org/10.1007/s10827-011-0374-4.
Weiler, N., Wood, L., Yu, J., Solla, S.A., Shepherd, G.M.G., 2008. Top-down laminar organization of the excitatory network in motor cortex. Nat. Neurosci. 11, 360–366.
Werner, G., Mountcastle, V.B., 1963. The variability of central neural activity in a sensory system, and its implications for the central reflection of sensory events. J. Neurophysiol. 26, 958–977.
White, J.A., Banks, M.I., Pearce, R.A., Kopell, N.J., 2000. Networks of interneurons with fast and slow gamma-aminobutyric acid type A (GABAA) kinetics provide substrate for mixed gamma–theta rhythm. Proc. Natl. Acad. Sci. 97, 8128–8133.
Whittington, M.A., Traub, R.D., Kopell, N., Ermentrout, B., Buhl, E.H., 2000. Inhibition-based rhythms: experimental and mathematical observations on network dynamics. Int. J. Psychophysiol. 38, 315–336.
Yoshimura, Y., Dantzker, J.L., Callaway, E.M., 2005. Excitatory cortical neurons form fine-scale functional networks. Nature 433, 868–873.
Yuan, K., Fink, K.L., Winer, J.A., Schreiner, C.E., 2011. Local connection patterns of parvalbumin-positive inhibitory interneurons in rat primary auditory cortex. Hear. Res. 274, 121–128.
Zhang, Y., Wang, X., Bressler, S.L., Chen, Y., Ding, M., 2008. Prestimulus cortical activity is correlated with speed of visuomotor processing. J. Cogn. Neurosci. 20, 1915–1925.